THE JOURNAL OF PHYSICAL CHEMISTRY A
A JOURNAL OF THE AMERICAN CHEMICAL SOCIETY

pubs.acs.org/JPCA

Article

Kinetic and Products Study of the Atmospheric Degradation of *trans*-2-Hexenal with Cl Atoms

Published as part of The Journal of Physical Chemistry virtual special issue "Advances in Atmospheric Chemical and Physical Processes".

Asma Grira,* María Antiñolo,* André Canosa, Alexandre Tomas, Gisèle El Dib, and Elena Jiménez

Cite This: *J. Phys. Chem. A* 2022, 126, 6973−6983

Read Online

ACCESS | Metrics & More | Article Recommendations | Supporting Information

ABSTRACT: The gas-phase reaction between *trans*-2-hexenal (T2H) and chlorine atoms (Cl) was studied using three complementary experimental setups at atmospheric pressure and room temperature. In this work, we studied the rate constant for the titled oxidation reaction as well as the formation of the gas-phase products and secondary organic aerosols (SOAs). The rate constant of the T2H + Cl reaction was determined using the relative method in a simulation chamber using proton-transfer reaction time-of-flight mass spectrometry (PTR-ToF-MS) to monitor the loss of T2H and the reference compound. An average reaction rate constant of $(3.17 \pm 0.72) \times 10^{-10}$ cm^3 molecule^{-1} s^{-1} was obtained. From this, the atmospheric lifetime of T2H due to Cl reaction was estimated to be 9 h for coastal regions. HCl, CO, and butanal were identified as primary products using Fourier transform infrared spectroscopy (FTIR). The molar yield of butanal was (6.4 ± 0.3)%. Formic acid was identified as a secondary product by FTIR. In addition, butanal, 2-chlorohexenal, and 2-hexenoic acid were identified as products by gas chromatography coupled to mass spectrometry but not quantified. A reaction mechanism is proposed based on the observed products. SOA formation was observed by using a fast mobility particle sizer spectrometer. The measured SOA yields reached maximum values of about 38% at high particle mass concentrations. This work exhibits for the first time that T2H can be a source of SOA in coastal atmospheres, where Cl concentrations can be high at dawn, or in industrial areas, such as ceramic industries, where Cl precursors may be present.

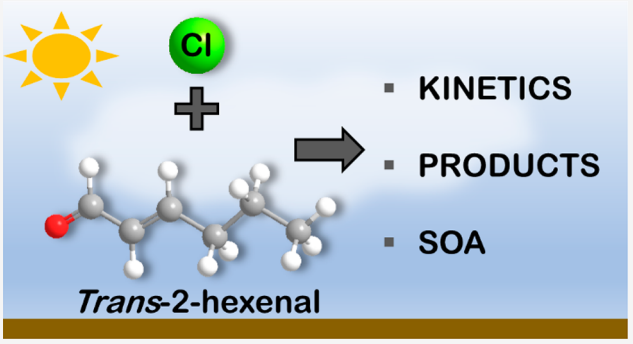

INTRODUCTION

Unsaturated C_6 aldehydes are widely emitted by fresh leaves,[1] vegetables,[2,3] and fruits.[4−6] These compounds could also be distributed through insect secretions to distance or attract other species from their surroundings.[7,8] Recent studies show that unsaturated C_6 aldehydes have been detected in the cooking fumes of the deep-frying process (150−200 °C) using cooking oils like coconut, safflower, canola, and extra virgin olive oils.[9−12] *Trans*-2-Hexenal (T2H) is one of these biogenic unsaturated C_6 aldehydes, which was detected from several sources.[13−17] T2H could be produced from damaged or wounded leaves as a product of the enzymatic activity of hydroperoxide lyase, a component of the lipoxygenase pathway.[7] T2H emissions from wounded leaves were demonstrated for tea leaves[18] and tomatoes.[19] Damaged plants may react by releasing T2H to induce its self-defense and/or to repair the damages.

Once T2H is released into the atmosphere, it is subjected to oxidation reactions, which proceed through hydrogen atom abstraction mainly from the carbonyl group or addition of the oxidant to the double bond. Hydroxyl (OH) radicals are the main T2H oxidant in the troposphere during daytime[20−22] and NO_3 radicals are during night-time,[23] while the O_3 reaction has been shown to be of minor importance.[24,25] Besides, the oxidation of T2H by chlorine (Cl) atoms could be a competitive oxidation channel, especially in the marine boundary layer (MBL) of coastal environments at dawn and in the Arctic troposphere during springtime, where the average [Cl]/[OH] ratio could be 1000 times higher than that at usual conditions.[26] Therefore, the oxidation process of T2H initiated by Cl may enrich the overall budget of free radicals, tropospheric ozone, and other secondary pollutants in the MBL.[27] To the best of our knowledge, no experimental

Received: July 18, 2022
Revised: September 15, 2022
Published: September 27, 2022

https://doi.org/10.1021/acs.jpca.2c05060
J. Phys. Chem. A 2022, 126, 6973−6983

reaction product study for the T2H + Cl reaction has been found in the literature that confirmed the formation of secondary gaseous pollutants and/or fine particles, the so-called secondary organic aerosols (SOAs).

While the rate constants of the oxidation reaction of T2H with OH radicals, O_3, and NO_3 radicals have been reported in several previous works,[20−23,25,28−35] the reactivity of T2H with Cl atoms has been scarcely studied. To the best of our knowledge, the only experimental study is from Rodríguez et al.[36] who studied the kinetics at room temperature and atmospheric pressure (air or N_2) using a relative method and found a rate constant of $(1.92 \pm 0.22) \times 10^{-10}$ cm^3 molecule^{-1} s^{-1}. This rate constant is surprisingly lower than the one for *trans*-2-pentenal (T2P) determined in our previous work ($(2.56 \pm 0.83) \times 10^{-10}$ cm^3 molecule^{-1} s^{-1}, ref 25), despite it containing less potential reaction sites than T2H. Moreover, Rodríguez et al.[36] is also lower than the one estimated by the SAR (structure−activity relationship) method (3.47×10^{-10} cm^3 molecule^{-1} s^{-1}) developed by Teruel et al.[37] Thus, in the present paper, the kinetics of the Cl-initiated reaction of T2H at atmospheric pressure and room temperature is revisited.

Regarding the reaction mechanism, a theoretical study by Shashikala and Janardanan[38] recently reported the most likely reaction channels for the first-step reaction in the degradation mechanisms of T2H by tropospheric oxidants (OH, NO_3, Cl, and O_3). These authors found that the reaction of T2H with Cl atoms presented the lowest energy barrier among all oxidants. Also, Shashikala and Janardanan noticed that the H-abstraction reaction from the aldehydic group in T2H was favored against the α- or β-addition to the double bond for the T2H reactions with OH and NO_3.

In the present work, the gas-phase reaction products of the T2H + Cl reaction are identified and quantified for the first time using FTIR spectroscopy and gas chromatography coupled to mass spectrometry (GC-MS), allowing a reaction mechanism to be proposed. Submicron particles can also be formed in the T2H + Cl gas-phase reaction. Knowing that particle size distributions of these particles are of great interest in the study of ambient aerosols, in the present work, the formation of SOAs with electrical mobility diameter between 5.6 and 560 nm has been monitored using a fast mobility particle sizer (FMPS), reporting SOA mass yields for the first time. The atmospheric implications of the studied reaction are discussed in terms of the atmospheric lifetime of T2H and its contribution, based on the detected products, to local air pollution.

EXPERIMENTAL SYSTEMS, TECHNIQUES, AND PROTOCOLS

The work on the T2H + Cl reaction has been partially carried out at IMT Nord Europe in Douai (France) and UCLM in Ciudad Real (Spain). On the one hand, the kinetic measurements were conducted at IMT Nord Europe in an atmospheric simulation chamber (hereafter D-ASC) at 296 ± 2 K and 730 ± 20 Torr of purified air. The experimental system and procedure are briefly described in "Kinetic Study" and in detail in Turpin et al.[39] On the other hand, the product study was performed at UCLM in Ciudad Real at 296 ± 2 K and 760 ± 20 Torr of synthetic air using a borosilicate White-type cell of 16 L or an atmospheric simulation chamber (hereafter CR-ASC). This setup and the methodology used are succinctly described in "Product Study", since it has been detailed in Ballesteros et al.[40] In separate experiments, the 16-L White cell was connected, in a closed circuit, to the CR-ASC and an FMPS spectrometer (TSI 3091) for carrying out the SOA formation study. This apparatus, procedure, and methodology were previously described in detail elsewhere[25,41] but are concisely explained below in "Monitoring Ultrafine Particles and Determination of the SOA Yield".

Kinetic Study. *Methodology and Experimental Conditions.* The Cl kinetics were performed using the relative method in the D-ASC chamber consisting of a 300 L Teflon bag coupled to a proton-transfer time-of-flight mass spectrometer, PTR-ToF-MS (Kore 2e), for monitoring the signals of T2H and isoprene as a reference compound as a function of time. The two following reactions occur simultaneously in the chamber:

$$\text{T2H} + \text{Cl} \xrightarrow{k_{\text{T2H}}} \text{Products} \quad \text{(R1)}$$

$$\text{Isoprene} + \text{Cl} \xrightarrow{k_{\text{Iso}}} \text{Products} \quad \text{(R2)}$$

where k_{T2H} and k_{Iso} are the rate constants for T2H + Cl and isoprene + Cl reactions, respectively.

In the PTR-ToF-MS, T2H ($C_6H_{10}O$) and isoprene (C_5H_8) react with a hydronium ion (H_3O^+), leading to the molecular ions $C_6H_{10}O{\cdot}H^+$ (m/z = 99, for T2H) and $C_5H_8{\cdot}H^+$ (m/z = 69, for isoprene) and several protonated fragments: $C_4H_8{\cdot}H^+$ (m/z = 57) and $C_6H_8{\cdot}H^+$ (m/z = 81) for T2H and $C_3H_4{\cdot}H^+$ (m/z = 41) for isoprene. The fragment $C_3H_4{\cdot}H^+$ was not used, since its behavior was very different from the $C_5H_8{\cdot}H^+$ fragment.

Figure S1 displays an example of the T2H and isoprene fragment evolution during a generic experiment. The experimental procedure started by injecting T2H in the reactor and following its concentration by the PTR-ToF-MS for 40 min in the dark (Figure S1, t = 55−95 min). Then, isoprene was added to the reactor and allowed to homogenize for 30 min (Figure S1, t = 95−125 min). During that time, two UV actinic lamps (Philips TLK-40 W/05 and Sylvania Blacklight, λ_{max} = 365 nm) were turned on to quantify the losses of T2H and isoprene by photolysis. Then, UV lights were turned off, and molecular chlorine (Cl_2) was added to the reaction mixture and left for 25 min in the chamber (Figure S1, t = 125−150 min). T2H and isoprene losses were evaluated during the described steps to check for possible adsorption on the D-ASC walls, UV photolysis, and/or a dark reaction with Cl_2. Negligible losses were observed for both T2H and isoprene with a ratio of the standard deviation to the mean value of the concentration within ∼45 min of measurements of less than 1.1%. Then, the lamps were switched on for 30 to 40 min in the presence of the T2H + isoprene + Cl_2 mixture (Figure S1, t = 150−190 min). At the end of each experiment, the reactor was cleaned by filling it with air and pumping it up several times.

The initial concentrations of T2H and isoprene in the D-ASC chamber were determined by a Fourier transform infrared, FTIR, spectrometer (Nicolet 6700 Thermo Fisher) using the IR spectral features in the 1182−1116 cm^{-1} range for T2H and in the 943−844 cm^{-1} range for isoprene. The quantification was done by using a reference spectrum of each reagent. The initial concentration of Cl_2 was calculated based on its injected volume into the chamber as explained in eq S1. The initial concentrations of T2H, isoprene, and Cl_2 were in the ranges $(5.9−11.6) \times 10^{13}$ molecules cm^{-3}, $(6.4−13.3) \times$

https://doi.org/10.1021/acs.jpca.2c05060
J. Phys. Chem. A 2022, 126, 6973−6983

10^{13} molecules cm^{-3}, and $(14.5-58.3) \times 10^{13}$ molecules cm^{-3}, respectively.

Determination of the Rate Constant k_{T2H}. In the presence of Cl atoms, the relative disappearance rates of T2H and isoprene were measured. The time evolution of the concentrations of T2H and the reference compound is described by the following expression, since there are no secondary loss processes:

$$\ln\left(\frac{[T2H]_0}{[T2H]_t}\right) = \frac{k_{T2H}}{k_{Iso}} \times \ln\left(\frac{[Iso]_0}{[Iso]_t}\right) \quad (1)$$

$[T2H]_0$, $[Iso]_0$ and $[T2H]_t$, $[Iso]_t$ are the concentrations of T2H and isoprene at reaction times $t = 0$ and t, respectively. The ratio of rate constants k_{T2H}/k_{Iso} was obtained by plotting $\ln([T2H]_0/[T2H]_t)$ versus $\ln([Iso]_0/[Iso]_t)$. k_{T2H} is then derived from the slope of such plots considering k_{Iso} as $(4.6 \pm 0.9) \times 10^{-10}$ cm^3 $molecule^{-1}$ s^{-1}, which is the weighted average of three values found in the literature[42−44] (see Table S2). k_{Iso} and the overall error (Δk_{Iso}) were calculated using eqs S2−S4. In this work, we considered Δk_{Iso} as twice the standard deviation of the weighted average k_{Iso}, $2\sigma_{<kIso>}$.

The overall error in k_{T2H}, Δk_{T2H}, was calculated according to eq S5 and it comprises statistical errors, Δk_{T2H}(stat), and systematic errors, Δk_{T2H}(syst). Δk_{T2H}(stat) was calculated according to eq S6, and Δk_{T2H}(syst) was estimated to be 10%.

Product Study. *Procedure and Experimental Conditions.* The experimental procedure started with the injection of T2H in the reactor (16-L or 264-L CR-ASC). In the 16-L reactor, the concentration of T2H was determined using FTIR spectroscopy (Nicolet Nexus 870, Thermo) based on a reference IR spectrum. IR spectra were recorded every 2 min with a resolution of 2 cm^{-1} in the IR spectral range 4000−650 cm^{-1} by accumulating 32 interferograms. In separate experiments in CR-ASC, the solid phase micro extraction (SPME)/GC-MS technique was used. In these experiments, a 50/30 μm divinylbenzene/Carboxen polydimethylsiloxane fiber (Supelco) was inserted every 15 min in the CR-ASC to absorb analytes for 5 min and injected in the GC-MS (Trace GC Ultra and DSQ II, Thermo Electron) equipped with a BPX35 column (30 m × 0.25 mm ID × 0.25 μm, SGE Analytical Science) working at a temperature ramp that ranged between 40 and 250 °C.

Actinic lamps (Philips Actinic BL TL 40W/10 1SL/25 (16-L reactor) and Philips TLK − 40 W/05 (CR-ASC), λ = 340−400 nm) were used to irradiate the gas sample with UV radiation, which generate Cl atoms from Cl_2 photolysis. In both reactors, after stabilization for 30 min, UV lights were turned on for 30 min to test the stability of T2H under photolysis conditions. Cl_2 was then added to the reactor, and the reaction mixture (synthetic air + T2H + Cl_2) was left to stabilize for 30 min in the dark. The loss rate constant of T2H due to heterogeneous and dark reactions and UV photolysis was on the same order of magnitude ($<4 \times 10^{-5}$ s^{-1}). Finally, when UV lights were turned on, the T2H + Cl reaction began, and the gaseous products formed were monitored for 60 min. The concentrations of T2H and Cl_2 used for the product studies are summarized in Table 1.

Determination of the Product Yield (Y_{Prod}). Two types of products can be distinguished: primary products directly formed through the T2H + Cl oxidation reaction and secondary products generated by primary product degradation. The product yield (Y_{Prod}) of a primary product is defined as the ratio of its concentration formed at a certain reaction time in the T2H + Cl reaction, [Prod], to that of the consumed reactant, Δ[T2H], over the same time scale according to eq 2.

$$Y_{Prod}(\%) = \frac{[Prod]}{\Delta[T2H]} \times 100 \quad (2)$$

Therefore, the [Prod] vs Δ[T2H] plot must be linear to guaranty that the product has a primary origin, and the slope represents Y_{Prod}.

Table 1. Experimental Conditions and Techniques Used during the Product Study

reactor (number of runs)	analytical technique	number of lamps (model)	compound	initial concentration range (10^{14} molecules cm^{-3})
16-L (7)	FTIR	3 (Philips Actinic BL TL 40 W/10 1SL/25)	T2H	4.7−22
			Cl_2	3.8−13
CR-ASC (2)	SPME/GC-MS	8 (Philips TLK−40 W/05)	T2H	6.2−6.3
			Cl_2	4.1

Monitoring Ultrafine Particles and Determination of the SOA Yield. To monitor the particle formation in the T2H + Cl reaction, the CR-ASC, the 16-L reactor, and the FMPS spectrometer were coupled. The FMPS spectrometer analyzes the particle number size distribution (electrical mobility diameters between 5.6 and 560 nm with a time resolution of 1 s) averaged over 1 min. The initial concentrations of T2H and Cl_2 were in the ranges $(0.8-2.7)\times10^{14}$ molecules cm^{-3} and $(1.3-7.2)\times10^{14}$ molecules cm^{-3}, respectively.

The procedure was as follows: the gas mixture was recirculated in a closed circuit allowing the gases to mix in the system. The system allows to simultaneously monitor the loss of T2H by in situ IR in the 16-L chamber and the FMPS sampling. The gas mixture flows from the CR-ASC to the FMPS through a 1 μm cut cyclone at a 10 L min^{-1} flow rate (which is the sampling flow rate of the instrument), and the filtered exhaust from the FMPS was then directed to the 16-L reactor where IR measurements were performed every 2 min by means of the FTIR spectrometer described in section "Kinetic Study". Then, the gas mixture comes back to the CR-ASC closing the circuit. Indeed, due to the high sampling flow rate of the FMPS, it cannot be directly connected to the 16-L chamber. This system was previously used in the study of the T2P + Cl reaction by Grira et al.[25]

The total time scale of the experiment was typically 80 min. In the first 10 min, the reaction mixture (synthetic air + T2H + Cl_2) was left in the dark, and the potential T2H wall losses and reaction with Cl_2 were estimated. While no reaction between T2H and Cl_2 was observed, a T2H wall loss constant $k_{L,T2H}$ of $<4 \times 10^{-5}$ s^{-1} was determined in the dark. $k_{L,T2H}$ was determined from the decay of [T2H] as exemplified in Figure S2a. Once the lamps surrounding the CR-ASC were turned on, the Cl reaction started, and T2H consumption and SOA formation were monitored for typically 50 min. SOA wall losses onto the reactor walls and/or through the filters of the FMPS, $k_{L,SOA}$, were evaluated leaving the reaction mixture for typically 20 min in the dark, after the end of the reaction. This parameter was obtained from the decay of the mass concentrations of particles (M_{SOA}) shown in the example depicted in Figure S2b. M_{SOA} was calculated using the measured particle number size distributions assuming spherical geometry and a particle density of 1.4 g cm^{-3} (recommended

https://doi.org/10.1021/acs.jpca.2c05060
J. Phys. Chem. A 2022, 126, 6973−6983

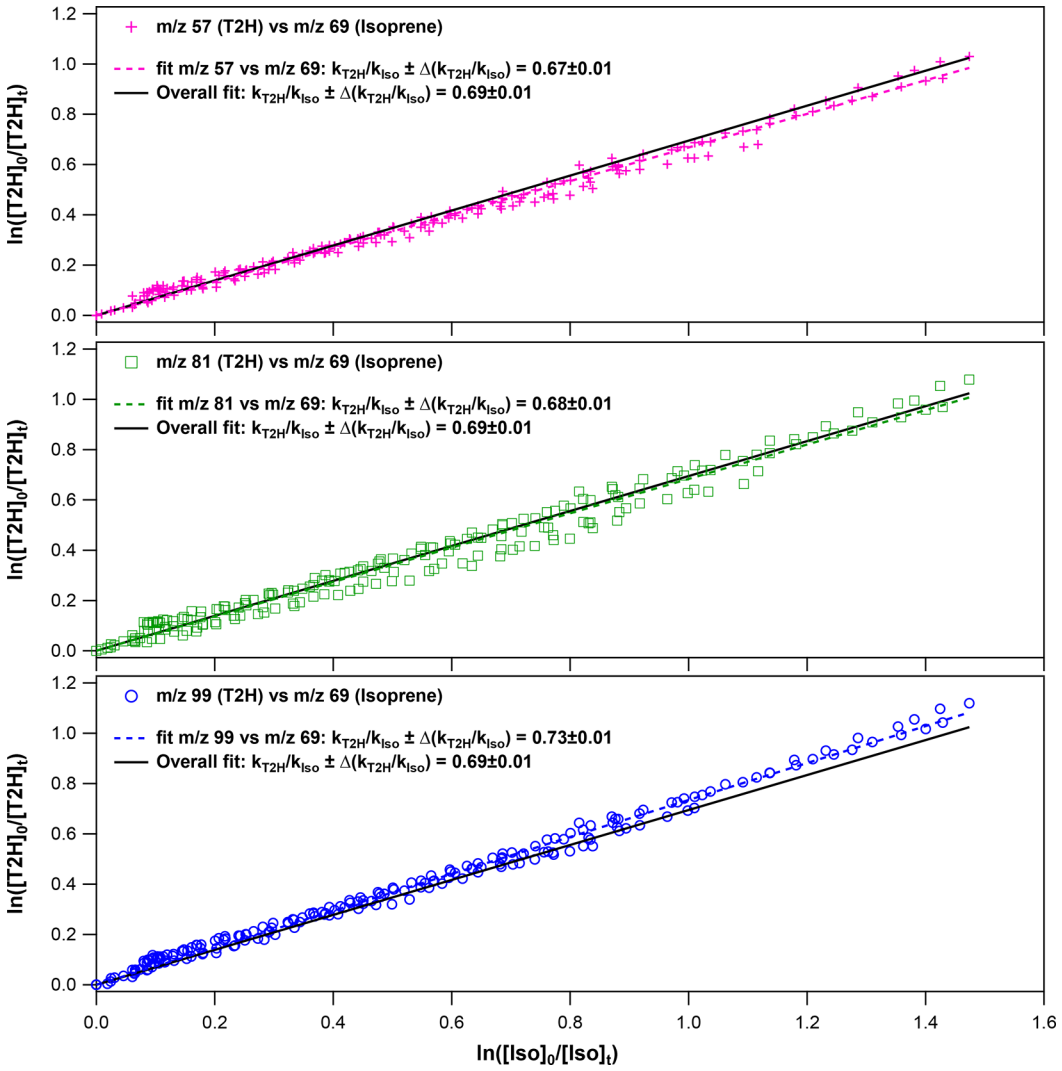

Figure 1. Plots of the decay of [T2H] vs that of [isoprene] in the presence of Cl for each observed peak of T2H. The continuous black line in each panel shows the linear regression of the combined data from the three series.

Table 2. Summary of the Rate Constants for the Reactions of a Series of C_3-C_7 Alkenals with Cl Atoms at Room Temperature and Atmospheric Pressure

unsaturated aldehyde (linear formula)	k (10^{-10} cm^3 molecule^{-1} s^{-1})	technique[a]	reference
2-propenal or acrolein (CH_2=CH–CHO)	2.2 ± 0.3	GC-FID	Thévenet et al.[47]
	2.2 ± 0.3	FTIR	Canosa-Mas et al.[48]
	1.8 ± 0.3	FTIR	Ullerstam et al.[49]
	2.5 ± 0.7	GC-FID	Wang et al.[50]
2-methyl-2-propenal or methacrolein (CH_2=C(CH_3)–CHO)	3.2 ± 0.5	FTIR	Canosa-Mas et al.[48]
	2.9 ± 0.8	GC-FID	Wang et al.[50]
trans-2-butenal or crotonaldehyde (*trans*-CH_3–CH=CH–CHO)	2.6 ± 0.3	GC-FID	Thévenet et al.[47]
	2.2 ± 0.4	FTIR	Ullerstam et al.[49]
	3.2 ± 0.9	GC-FID	Wang et al.[50]
trans-2-methyl-2-butenal (*trans*-CH_3–CH=C(CH_3)–CHO)	2.45 ± 0.32	FTIR	Antiñolo et al.[41]
trans-2-pentenal (*trans*-CH_3–CH_2–CH=CH–CHO)	1.31 ± 0.19	GC-FID	Rodríguez et al.[36]
	3.47	SAR estimation	this work
	2.56 ± 0.83	FTIR	Grira et al.[25]
trans-2-hexenal (*trans*-CH_3–CH_2–CH_2–CH=CH–CHO)	1.92 ± 0.22	GC-FID	Rodríguez et al.[36]
	2.06 ± 0.46	re-evaluation in the present work	Rodríguez et al.[36]
	3.17 ± 0.72	PTR-MS	this work
trans-2-heptenal (*trans*-CH_3–CH_2–CH_2–CH_2–CH=CH–CHO)	2.40 ± 0.29	GC-FID	Rodríguez et al.[36]

[a]GC-FID: Gas chromatography-flame ionization detection; FTIR: Fourier transform infrared; PTR-MS: proton-transfer mass spectrometry.

https://doi.org/10.1021/acs.jpca.2c05060
J. Phys. Chem. A 2022, 126, 6973−6983

by Hallquist et al.[45]). The loss rate constant $k_{L,SOA}$ was measured to be in the range $(4.35-6.18) \times 10^{-4}$ s^{-1}. From the slope of M_{SOA} versus T2H consumption (Δ[T2H]) plots, as shown by eq 3, the SOA yield (Y_{SOA}) can be determined. Both M_{SOA} and Δ[T2H] were corrected as described in previous works, Antiñolo et al.[46] and Grira et al.,[25] taking into account $k_{L,T2H}$, and $k_{L,SOA}$.

$$Y_{SOA}(\%) = \frac{M_{SOA}}{\Delta[T2H]} \times 100 \quad (3)$$

Chemicals. The chemicals and gases employed in this work at IMT were the following ones (in bracket the purity and supplier are stated): T2H (98%, Sigma−Aldrich), isoprene (99%, Sigma−Aldrich), Cl_2 (10% in N_2, Air Products). At IMT, we used an extra pure zero air, which was produced with a pure air generator (AZ-2020, Claind) with relative humidity (RH) < 2 ppm, and CO and CO_2 < 80 ppb. At UCLM, T2H (98%, Sigma−Aldrich), Cl_2 (99.8%, Sigma−Aldrich), and synthetic air (99.999%, Air Liquide) was used.

RESULTS AND DISCUSSION

Rate Constant for the T2H + Cl Reaction. Figure 1 displays the obtained loss of T2H versus that of the reference compound in the presence of Cl atoms. The plot of $\ln([T2H]_0/[T2H]_t)$ versus $\ln([Iso]_0/[Iso]_t)$ displays a good linearity, and the ratios k_{T2H}/k_{Iso} are relatively consistent for the three masses of T2H used in the analysis (m/z = 99, m/z = 81, and m/z = 57). The reported slope k_{T2H}/k_{Iso} (0.69 ± 0.01) arises from a linear regression of the combined data from the three series. k_{T2H} was determined from k_{T2H}/k_{Iso} considering the k_{Iso} given in section "Kinetic Study":

$$k_{T2H} = (3.17 \pm 0.72) \times 10^{-10} \text{ cm}^3 \text{ molecule}^{-1} \text{ s}^{-1}$$

The overall error in the rate constant is 23% (see Supporting Information for a detailed explanation of the error analysis).

Comparison with Literature Data. Table 2 gathers the k_{T2H} obtained in this work on the T2H + Cl reaction and that reported by Rodríguez et al.[36] As it can be seen, this latter value of k_{T2H} is 39% lower than the present measurement. In Rodríguez et al.'s work, the monitoring of concentration of T2H and the reference compounds (ethane and propene) was carried out by GC coupled to a flame ionization detector (GC-FID). The source of the observed discrepancy is not due to Cl rate constants used by these authors for the reference compounds (k_{Ethane} and $k_{Propene}$). In 2009, IUPAC updated the recommended values of k_{Ethane} and $k_{Propene}$ for the rate constants of the Cl-initiated reactions of ethane and propene. This re-evaluation of k_{T2H} slightly changes the value by Rodríguez et al. by about 7%: $(2.06 \pm 0.46) \times 10^{-10}$ cm^3 $molecule^{-1}$ s^{-1}.

In Figure S3, a comparison between the rate constants determined in different studies for the Cl reaction of a series of C_3-C_7 alkenals is presented. It is noted that data from Rodríguez et al.[36] are systematically lower than other studies, indicating that they may probably have unaccounted systematic errors. Therefore, the source of the observed discrepancy is still unclear.

Structure−Activity Relationship (SAR). Using the method proposed by Teruel et al.,[37] which is based on a basic rate constant for the *trans*-RHC═CHR structure and some "group factors", the rate constant for the T2H + Cl can be estimated. Teruel et al.[37] provides the value of the group factor for −C(O)H but not for the $CH_3CH_2CH_2-$ group. Instead, the value for the CH_3CH_2- group is given. Since it is expected that the contribution of the $CH_3CH_2CH_2-$ group to the estimated k_{T2H} is higher than that of the CH_3CH_2- group, it is likely that the corresponding group factor is at least equal to the CH_3CH_2- one. Hence, a lower limit of the k_{T2H} estimated with the SAR method can be provided: $k_{T2H(SAR)} = 3.47 \times 10^{-10}$ cm^3 $molecule^{-1}$ s^{-1}. This number is very close to the experimental value reported here and 83% higher than that reported by Rodríguez et al.[36]

When comparing the Cl reactivity of linear unsaturated aldehydes, we observe that the rate constant for Cl reactions with C_3-C_7 alkenals seems to depend barely on the aldehyde chain length (Table 2 and Figure S3). As shown in Figure S3 and excluding the result for *trans*-2-heptenal reported by Rodríguez et al.,[36] the Cl rate coefficient increases by about 50% from 2-propenal (C_3) to *trans*-2-hexenal (C_6), even though there is some scattering in the literature values.

Comparing the Cl reactivity toward *trans*-2-butenal and *trans*-2-pentenal with that of branched unsaturated aldehydes with the same number of carbon atoms, such as 2-methyl-2-propenal and *trans*-2-methyl-2-butenal, we observed that the presence of the methyl group has no apparent effect on the reactivity. No data are available up to date to compare the reactivity of *trans*-2-hexenal with a branched unsaturated aldehyde with the same number of C atoms.

It would have been interesting to compare the reactivity of T2H toward Cl atoms with that of the corresponding alkene, since it has been postulated that alkenes and their corresponding unsaturated aldehydes react via similar Cl addition to the double bond.[51] Unfortunately, no data is available in the literature for the reaction of Cl with *trans*-2-hexene. Further experimental studies on alkenes + Cl reactions would be desirable.

Gaseous Reaction Products. *Temporal Evolution of Species in the Reaction Mixture. Detection by FTIR Spectroscopy.* As can be seen in Figure S4, IR features of HCl, CO, HC(O)OH, and butanal are present in the final spectrum. The IR spectral features used for this analysis were 1610−1750 cm^{-1} for T2H, 2600−3100 cm^{-1} for HCl, 2039−2239 cm^{-1} for CO, 2870−2950 cm^{-1} for HC(O)OH, and 2750−2660 cm^{-1} for butanal. The identification and the quantification of these products were made using reference IR spectra. After subtraction of the IR features of the products, the residual spectrum showed some peaks that indicate that there were unidentified products. The group of peaks between 3000 and 2700 cm^{-1} corresponds to C−H stretching vibrational modes. The most intense peak centered at 1750 cm^{-1} is typically assigned to C═O bonds, and the weak bands between 1500 and 1000 cm^{-1} can be due to C−C stretching or C−H bending modes. Figure 2 shows typical concentration vs time profiles for the consumption of T2H and the formation of the detected products.

Detection by SPME/GC-MS. As shown in Figure S5, the reaction products detected by GC-MS were butanal (retention time RT = 2.88 min), 2-chlorohexanal (RT = 4.84 min), and 2-hexenoic acid (RT = 6.36 min). They were identified by means of their electronic impact mass spectra. However, the signal from the GC-MS was not stable enough to allow for a reliable quantification of these species, and no internal standard was introduced in the gas mixture.

The products detected in this work are in agreement with those observed for the crotonaldehyde + OH reaction[44] and

https://doi.org/10.1021/acs.jpca.2c05060
J. Phys. Chem. A 2022, 126, 6973−6983

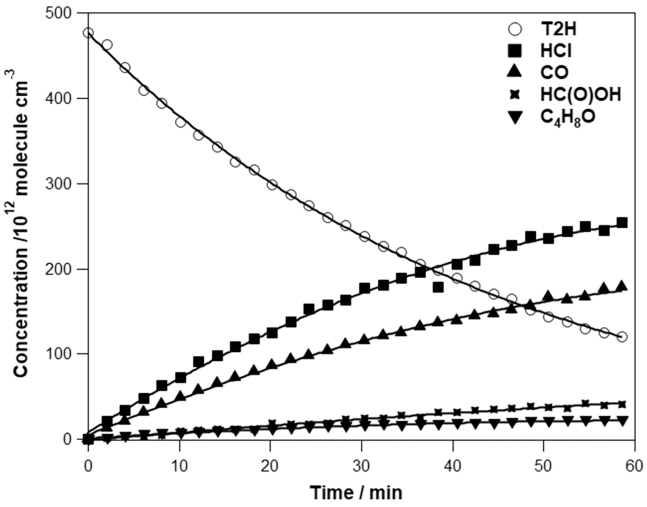

Figure 2. Concentration−time profile for T2H and the major products using $[T2H]_0 = 4.7 \times 10^{14}$ molecules cm^{-3} and $[Cl_2]_0 = 3.9 \times 10^{14}$ molecules cm^{-3}.

trans-2-pentenal + Cl reaction.[25] In all these reactions, the corresponding saturated aldehyde with two less C atoms and CO were formed.

Molar Yields of Reaction Products. The product yields were determined based on the quantified concentrations of T2H and products by FTIR spectroscopy as a function of time. Here, only the butanal yield is reported, since the other quantified products (HCl, CO, and HC(O)OH) are known to be very final products with a wide variety of sources, and their molar yields provide little information. The corresponding plot displaying [Butanal] vs Δ[T2H] according to eq 2 is shown in Figure 3. The overall errors on the formation yields (ΔY_{Prod})

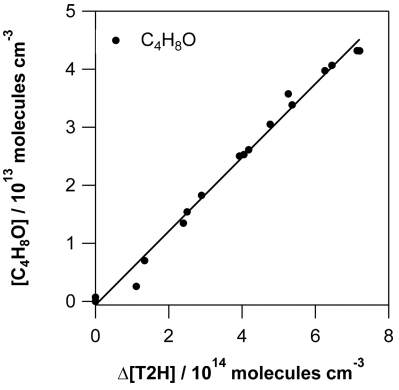

Figure 3. Product yield for butanal.

were calculated as described in eq S7. The molar yield of butanal obtained from the slope is (6.35 ± 0.30)%. The carbon mass balance was found to be more than 20% at the end of the reaction, if calculated considering the formation of butanal, CO, and HC(O)OH.

Proposed Reaction Mechanism. Based on previous experimental studies on the Cl reaction of unsaturated aldehydes[25,52] and the theoretical work of Shashikala and Janardanan on the T2H degradation,[38] the reaction is expected to proceed via three pathways: addition of the Cl atom to the C=C double bond, either to C_α or C_β, and abstraction of the hydrogen atom from the −C(O)H group. Shashikala and Janardanan[38] concluded that allylic H-abstraction is a minor reaction pathway; therefore, in this work, this route has not been considered. In Figure 4, the resulting reaction pathways that may support the observed products are displayed.

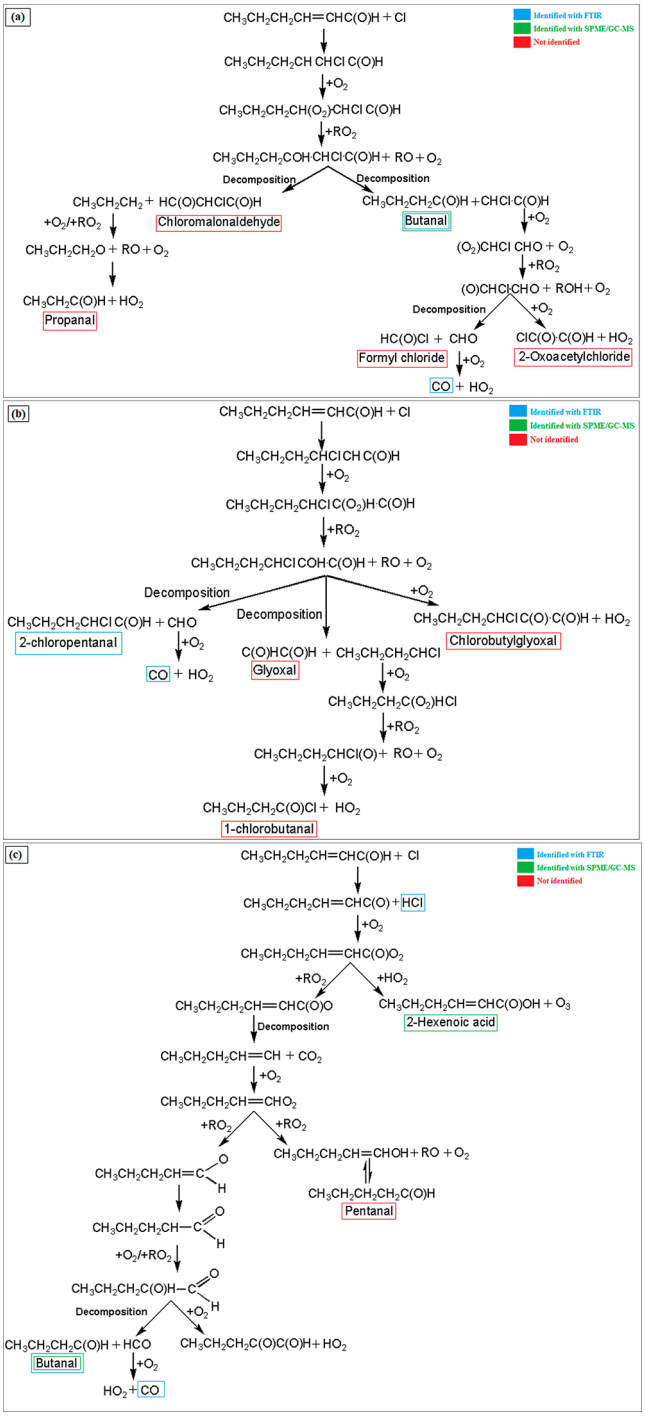

Figure 4. Proposed mechanisms for the reaction of T2H with a Cl atom: α-addition (a), β-addition (b), and H-abstraction (c).

As seen in Figure 4a, the α-addition forms the $CH_3CH_2CH_2CHCHClC(O)H$ radical, which can react with O_2/RO_2 to lead to the corresponding chloroalkoxy radical ($CH_3CH_2CH_2COHCHClC(O)H$). The decomposition of the chloroalkoxy radical leads to the formation of butanal ($CH_3CH_2CH_2C(O)H$) and, after further reactions, 2-oxoacetyl chloride (ClC(O)C(O)H) and formyl chloride (HC(O)-

https://doi.org/10.1021/acs.jpca.2c05060
J. Phys. Chem. A 2022, 126, 6973−6983

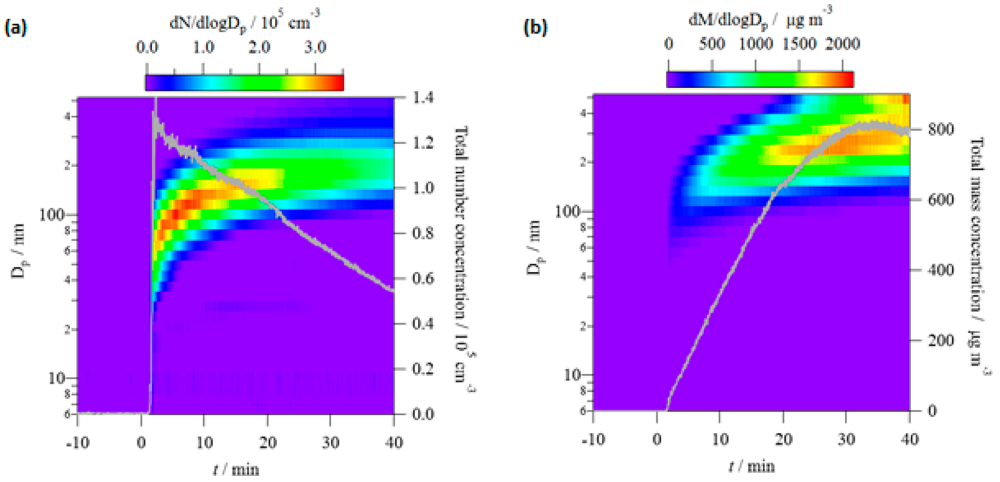

Figure 5. Typical time-dependent size distributions for SOA from T2H + Cl measured by the FMPS in terms of (a) particle number concentrations and (b) particle mass concentrations, considering a mass density of 1.4 g cm^{-3}. Initial concentrations were 2.7 × 10^{14} and 6.5 × 10^{14} molecules cm^{-3} for T2H and Cl_2, respectively. Time zero corresponds to the start of the reaction. The gray line represents the temporal evolution of the total (a) number concentration and (b) mass concentration.

Cl). CO is also formed as a coproduct of formyl chloride. The second channel leads to the formation of propanal ($CH_3CH_2C(O)H$) and chloromalonaldehyde (HC(O)-CHClC(O)H), which were not detected.

In Figure 4b, the β-addition mechanism proceeds through the formation of the $CH_3CH_2CH_2CHClCHC(O)H$ radical, which can react with O_2/RO_2 to lead to the $CH_3CH_2CH_2CHClCOHC(O)H$ radical. This radical may decompose to lead to the formation of 2-chloropentanal ($CH_3CH_2CH_2CHClC(O)H$) and CO, identified by FTIR. As shown in Figure 4b, the $CH_3CH_2CH_2CHClCOHC(O)H$ radical may also lead to the formation of glyoxal (C(O)HC-(O)H), 1-chlorobutanal ($CH_3CH_2CH_2C(O)Cl$), and chlorobutylglyoxal ($CH_3CH_2CH_2CHClC(O)C(O)H$), which were not detected in this work, suggesting that either these channels do not occur or these routes are minor with respect to others.

In Figure 4c, the H-abstraction from the formyl group leads to the formation of the $CH_3CH_2CH_2CH{=}CHC(O)$ radical and HCl, identified by FTIR. In the presence of O_2, the $CH_3CH_2CH_2CH{=}CHC(O)$ radical may be transformed to the acylperoxy radical $CH_3CH_2CH_2CH{=}CHC(O)O_2$, which produces 2-hexenoic acid ($CH_3CH_2CH_2CH{=}CHC(O)OH$) (identified by GC-MS) and ozone in the presence of HO_2. The $CH_3CH_2CH_2CH{=}CHC(O)O_2$ radical may also react with RO_2 and produce the $CH_3CH_2CH_2CH{=}CHC(O)O$ radical, which decomposes rapidly into CO_2 and the $CH_3CH_2CH_2CH{=}CH$ radical. The latter is converted to $CH_3CH_2CH_2CH{=}CHO_2$ in the presence of O_2 further reacting with RO_2 to generate pentanal $CH_3CH_2CH_2CH_2C$-(O)H (not identified), butanal $CH_3CH_2CH_2C(O)H$ (identified by FTIR and GC-MS and quantified by FTIR), and CO (identified by FTIR).

In the three proposed routes, the RO_2 radicals can undergo autoxidation leading to the formation of peroxides and hydroperoxides that are highly oxygenated organic molecules (HOMs). The RO_2 autoxidation reaction consists of an intramolecular H-abstraction or a H-shift, that generates an alkyl radical, R, with a hydroperoxyl functional group (−OOH). For example, in the Cl + T2H reaction, the first RO_2 radical formed in Figure 4a can be autoxidized to

$$CH_3CH_2CH_2CH(OO)CHClC(O)H \rightarrow CH_3CH_2CH_2CH(OOH)CHClC(O) \quad (R3)$$

The $CH_3CH_2CH_2CH(OOH)CHClC(O)$ radical can further react with O_2 to form a new, more oxidized, RO_2:

$$CH_3CH_2CH_2CH(OOH)CHClC(O) + O_2 \rightarrow CH_3CH_2CH_2CH(OOH)CHClC(O)O_2 \quad (R4)$$

The $CH_3CH_2CH_2CH(OOH)CHClC(O)O_2$ radical will further react probably leading to the formation of HOMs. HOMs are known to condense easily due to their low vapor pressure and could not be detected in this work but they may contribute to particle formation.

In the proposed mechanism, since CO is formed from the three channels, and butanal is part of the α-addition and the H-abstraction routes, these compounds are not of great help to quantify the relative contributions of addition and abstraction channels. On the other hand, HCl and 2-hexenoic acid were observed only in H-abstraction. However, HCl can also be issued from other abstraction reactions occurring in the reactor, and then, its yield may not reflect the one of the T2H + Cl reaction alone. The experimental observations, nevertheless, indicate that all three channels should be open. Although formic acid has been identified in the present work, it does not appear in the three suggested mechanisms. Therefore, it is likely that it is generated from secondary processes in the reactor.

Particle Formation. *Particle Size Distribution and Total Number Concentration.* A typical temporal evolution of the particle size distribution, in terms of normalized particle number concentrations (dN/dlogDp) is displayed in Figure 5a for given initial concentrations of T2H and Cl_2. In this example, at t = 2 min, the first particles appeared rapidly reaching a total number concentration (N_p) around 1.4 × 10^5 particles cm^{-3} with the maximum at about 70 nm diameter. From t = 2 min to t = 10 min, the diameter of the maximum grew from 70 to 143 nm, while N_p decreased down to 1.0 × 10^5 particles/cm^3. Finally, from t = 10 min to t = 40 min (end of the reaction), N_p decreased to 5.4 × 10^4 particles cm^{-3}, and the maximum diameter increased up to 221 nm. The

https://doi.org/10.1021/acs.jpca.2c05060
J. Phys. Chem. A 2022, 126, 6973−6983

coagulation of small particles explains the particle diameter growth versus time while the total number of particles decreases.

Particle Mass Concentrations. A typical temporal evolution of the normalized mass concentrations ($dM/d\log Dp$) is displayed in Figure 5b for the same initial concentrations as Figure 5a. In this example, the mass increase of the particles started 2 min after initiation of the T2H + Cl reaction. The mass concentrations of particles (M_{SOA}) reached a plateau after roughly 30 min of reaction and then started to decrease, probably due to losses in the system.

SOA Yields. For every experimental initial condition, it is possible to determine the SOA yield Y_{SOA} from the slope of the M_{SOA} linear increase as a function of the T2H consumption as illustrated in Figure 6. Such plots were obtained for many

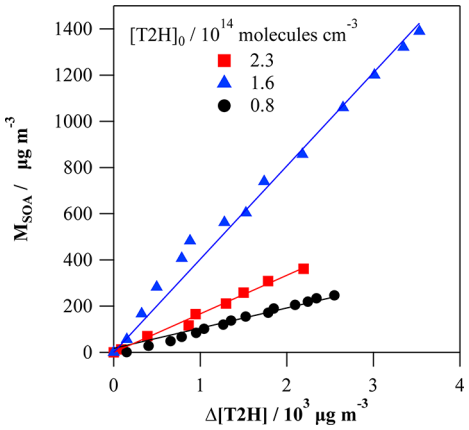

Figure 6. Examples of the produced SOA mass concentration M_{SOA} from the T2H + Cl reaction as a function of the consumed T2H (all initial concentrations of T2H and Cl_2 are indicated in Table 3).

different experimental conditions, and the SOA yields are given in Table 3 for each situation as well as the initial concentrations of T2H and Cl_2 ($[T2H]_0$ and $[Cl_2]_0$), the reacted T2H ($\Delta[T2H]$), and $M_{SOA,max}$.

Y_{SOA} for the T2H + Cl reaction has been found to range between 5 and 38%. These values are found to be higher than

Table 3. Experimental Conditions and Results Obtained for the SOA Study

$[T2H]_0$ (10^{-14} molecules cm^{-3})	$[Cl_2]_0$ (10^{-14} molecules cm^{-3})	$\Delta[T2H]$ (10^{-13} molecules cm^{-3})	$M_{SOA,max}$ (10^{-2} µg m^{-3})	% $Y_{SOA} \pm 2\sigma$
1.4	1.3	1.1	1.8	5.1 ± 0.8
2.1	2.6	2.3	3.9	9.8 ± 1.1
0.8	2.1	1.7	2.5	10.5 ± 0.4
1.9	3.1	1.6	5.9	13.0 ± 2.4
2.2	4.3	2.0	7.1	15.3 ± 1.0
2.3	3.8	1.3	3.6	16.9 ± 1.4
2.2	5	1.7	7.0	20.7 ± 5.5
2.7	6.5	1.0	4.9	27.7 ± 4.8
2.5	6	2.5	15.3	29.9 ± 4.2
2.1	4.9	0.71	6.6	31.0 ± 4.6
1.2	5.7	1.7	15.7	31.1 ± 5.8
2.0	7.2	1.4	12.9	33.1 ± 2.8
1.1	4.0	0.7	5.2	33.1 ± 7.5
1.6	6.8	2.1	14.9	37.5 ± 4.4

the results obtained for the Cl reaction of *trans*-2-pentenal, which were in the 1−7% range,[25] and *trans*-2-methyl-2-butenal, which were between 0.3 and 1.7%.[41] SOA yields in the range of 7 to 36%[53] were obtained for the reaction of Cl with isoprene being these SOA yields more similar to the values determined in the present work for the reaction of Cl with T2H.

Figure 7 shows the plot of Y_{SOA} versus $M_{SOA,max}$, and the fit of the data using the one-product model from Odum et al.[54] (eq 4).

$$Y_{SOA} = M_{SOA,max} \times \left(\frac{\alpha \times K_p}{1 + M_{SOA,max} \times K_p} \right) \quad (4)$$

where α is the mass-based gas-phase stoichiometric coefficient of a model product, and K_p represents its gas-particle partitioning equilibrium coefficient. A least-squares regression on the data gives the following parameters: $\alpha = (50.0 \pm 13.5)\%$ and $K_p = (1.3 \pm 0.7) \times 10^{-3}$ m^3 μg^{-1}. Uncertainties represent two standard deviations (2σ). α indicates that Y_{SOA} tends toward 50% at very high M_{SOA} values, which is higher than what was found for a similar reaction, T2P + Cl,[25] where α was 10%. On the other hand, K_p could indicate that the semivolatile species that produce the SOA formation are mostly in the vapor rather than the condensed phase, which is similar to what was observed for T2P + Cl ($K_p = (6.0 \pm 2.7) \times 10^{-4}$ m^3 μg^{-1}, ref 25). However, it must be noted that many products result from the oxidation of a VOC, so the parameters obtained from the fitting to eq 4 allow for easy comparison of yield curves, but as reported by Cai et al.,[55] the fitted parameters provide no specific information about the real oxidation products, and ascribing meaning to these is not recommended.

ATMOSPHERIC IMPLICATIONS AND CONCLUSIONS

As discussed by Jiménez et al.,[21] UV photodissociation of T2H in the solar actinic region is not a significant degradation process. Therefore, here we only consider the atmospheric lifetime (τ) of T2H due to the oxidation reactions with OH, Cl, O_3, and NO_3, which was estimated using the following equation:

$$\tau = \frac{1}{\sum_i (k_{Oxi} \times [Oxi])_i} \quad (5)$$

where k_{Oxi} is the rate constant for the reaction of the unsaturated aldehyde with the oxidant (i) and [Oxi] is the averaged atmospheric concentration of the oxidant for two situations: a global atmosphere and a coastal area. Globally, the 24 h average concentrations considered to estimate τ were: $[OH] = 1 \times 10^6$ radicals cm^{-3},[56] $[Cl] = 1 \times 10^3$ atoms cm^{-3},[57] $[O_3] = 7 \times 10^{11}$ molecules cm^{-3},[58] and $[NO_3] = 2.5 \times 10^8$ radicals cm^{-3}.[59] The individual atmospheric lifetimes calculated for every oxidant are summarized in Table 4. Globally, the depletion of T2H due to the Cl, O_3, and NO_3 reactions is negligible, since its individual lifetime is about 37, 10, and 3 days, respectively. As indicated in this table, the oxidation of T2H by OH reaction dominates the fate of T2H in the atmosphere with a lifetime τ_{OH} of 7 h. The overall lifetime calculated according to eq 5 is 6 h.

For the estimation of τ in the second scenario, the peak concentration measured at dawn in the marine boundary layer and polluted urban regions was used, $[Cl] = 1 \times 10^5$ atoms

https://doi.org/10.1021/acs.jpca.2c05060
J. Phys. Chem. A 2022, 126, 6973−6983

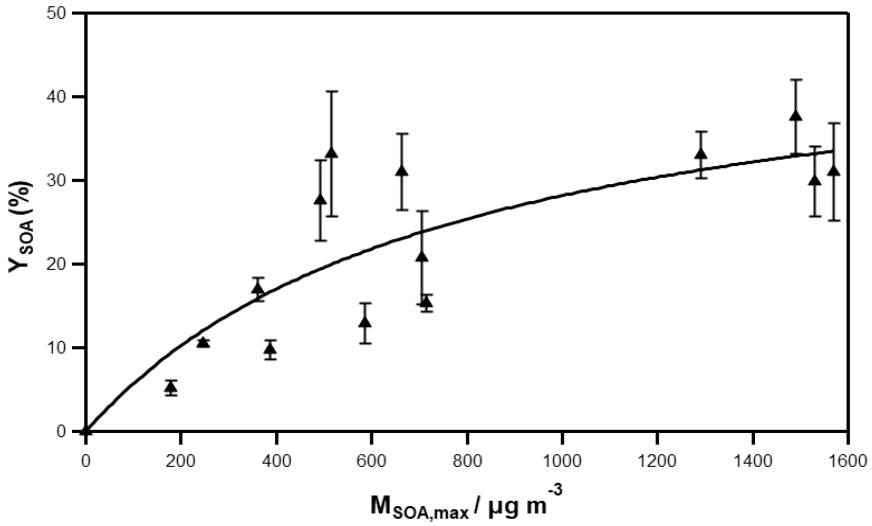

Figure 7. Plot of Y_{SOA} as a function of $M_{SOA,max}$ for the reaction between T2H and Cl according to the one-product model developed by Odum et al.[54] (eq 4).

Table 4. Estimated Atmospheric Lifetimes of T2H toward Atmospheric Oxidants (Cl, O_3, NO_3, and OH)

k_{Cl} (10^{-10} molecule^{-1} cm^3 s^{-1})	$\tau_{Cl\text{-}high}$ (h)	$\tau_{Cl\text{-}low}$ (days)	k_{O3} (10^{-18} molecule^{-1} cm^3 s^{-1})	τ_{O3} (days)	k_{NO3} (10^{-14} molecule^{-1} cm^3 s^{-1})	τ_{NO3} (days)	k_{OH} (10^{-11} molecule^{-1} cm^3 s^{-1})	τ_{OH} (h)
3.17 ± 0.72[a]	9	37	**1.66**[b]	10	**1.71**[c]	3[c]	**3.88**[d]	7[d]

[a]This work. [b]Average of Atkinson et al.,[23] Grosjean et al.,[28] Kalalian et al.,[29] and Grira et al.[25] (Table S3). [c]Average of Grosjean et al.,[30] Cabañas et al.,[31] Zhao et al.,[32] Kerdouci et al.,[33] and Rayez et al.[34] (Table S3). [d]Average of Grosjean et al.,[30] Atkinson et al.,[23] Albaladejo et al.,[35] Davis et al.,[22] Jiménez et al.[21] and Gao et al.[20] (Table S3).

cm^{-3}.[60] In this specific situation, $\tau_{Cl\text{-}high}$ is 9 h. Therefore, the T2H + Cl reaction becomes competitive with the OH reaction, since at dawn, where the solar flux is very low, the OH concentration is on the order of magnitude of Cl atoms, 10^5 radicals cm^{-3}.[58] The overall lifetime is 7 h in a chlorine enhanced concentration zone, with contributions of 10 and 77% of OH and Cl, respectively. Removal of T2H by NO_3 and O_3 are 10 and 3%, respectively, under this circumstance.

Regarding the impact of the T2H + Cl reaction on air quality, it may contribute to the local formation of secondary pollutants leading to the emission of free radicals (for example HO_2 was formed from the α,β-addition, and the H-abstraction pathways) in the atmosphere. In the absence of NOx, as reported for the first time in the present work, the T2H + Cl reaction may significantly contribute to the harmful SOA formed (yields of up to 38%). This study was carried under NOx-free conditions; however, further studies are required to evaluate the contribution of NOx to the atmospheric degradation of unsaturated aldehydes.

■ ASSOCIATED CONTENT

Supporting Information

The Supporting Information is available free of charge at https://pubs.acs.org/doi/10.1021/acs.jpca.2c05060.

Equations used in this work, figures concerning the kinetic and product studies, and tables summarizing rate constants (PDF)

■ AUTHOR INFORMATION

Corresponding Authors

Asma Grira − *CNRS, IPR (Institut de Physique de Rennes)−UMR 6251, Université de Rennes, F-35000 Rennes, France; IMT Nord Europe, Institut Mines−Télécom, Univ. Lille, Center for Energy and Environment, F-59000 Lille, France*; Phone: + 33 3 27 71 26 29; Email: asma.grira@imt-nord-europe.fr

María Antiñolo − *Departamento de Química Física, Facultad de Ciencias y Tecnologías Químicas, Universidad de Castilla−La Mancha, 13071 Ciudad Real, Spain; Instituto de Investigación en Combustión y Contaminación Atmosférica (ICCA), Universidad de Castilla−La Mancha, 13071 Ciudad Real, Spain*; orcid.org/0000-0001-6769-0470; Phone: +34 9 26 29 53 00; Email: maria.antinolo@uclm.es

Authors

André Canosa − *CNRS, IPR (Institut de Physique de Rennes)−UMR 6251, Université de Rennes, F-35000 Rennes, France*; orcid.org/0000-0001-5719-9899

Alexandre Tomas − *IMT Nord Europe, Institut Mines−Télécom, Univ. Lille, Center for Energy and Environment, F-59000 Lille, France*; orcid.org/0000-0002-0125-581X

Gisèle El Dib − *CNRS, IPR (Institut de Physique de Rennes)−UMR 6251, Université de Rennes, F-35000 Rennes, France*

Elena Jiménez − *Departamento de Química Física, Facultad de Ciencias y Tecnologías Químicas, Universidad de Castilla−La Mancha, 13071 Ciudad Real, Spain; Instituto de Investigación en Combustión y Contaminación Atmosférica (ICCA), Universidad de Castilla−La Mancha, 13071 Ciudad Real, Spain*; orcid.org/0000-0002-6302-0346

Complete contact information is available at: https://pubs.acs.org/10.1021/acs.jpca.2c05060

https://doi.org/10.1021/acs.jpca.2c05060
J. Phys. Chem. A 2022, 126, 6973−6983

Notes

The authors declare no competing financial interest.

■ ACKNOWLEDGMENTS

The authors are grateful to the INSU-LEFE French program, the International Emerging Action program funded by CNRS France (Cingaz project), and the Brittany Council. IMT Nord Europe acknowledges funding by the French ANR agency under contract No. ANR−11−LabX−0005−01 CaPPA (Chemical and Physical Properties of the Atmosphere), the Region Hauts−de−France, the Ministère de l'Enseignement Supérieur et de la Recherche (CPER Climibio), and the European Fund for Regional Economic Development. This research was also funded by the Consejería de Educación, Cultura y Deportes de la Junta de Comunidades de Castilla−La Mancha through the project SBPLY/19/180501/000052, and the University of Castilla−La Mancha (UCLM) through the projects 2020−GRIN−29016 and 2021−GRIN−31279 (Ayudas para la financiación de actividades de investigación dirigidas a grupos). M. Antiñolo acknowledges UCLM ∼ Plan Propio de Investigación for funding her research contract.

■ REFERENCES

(1) Hatanaka, A. The Fresh Green Odor Emitted by Plants. *Food Rev. Int.* **1996**, *12* (3), 303−350.
(2) Bourel, G.; Nicaud, J.-M.; Nthangeni, B.; Santiago-Gomez, P.; Belin, J.-M.; Husson, F. Fatty Acid Hydroperoxide Lyase of Green Bell Pepper: Cloning in Yarrowia Lipolytica and Biogenesis of Volatile Aldehydes. *Enzyme Microb. Technol.* **2004**, *35* (4), 293−299.
(3) Takeoka, G. Flavor Chemistry of Vegetables. *Flavor chemistry* **1999**, 287−304.
(4) Gray, D. A.; Prestage, S.; Linforth, R. S.; Taylor, A. J. Fresh Tomato Specific Fluctuations in the Composition of Lipoxygenase-Generated C_6 Aldehydes. *Food Chem.* **1999**, *64* (2), 149−155.
(5) Flavor and Aroma of Fresh-Cut Fruits and Vegetables. *Fresh-Cut Fruits and Vegetables: Science, Technology, and Market*; Lamikanra, O., Ed.; CRC Press, 2002; pp 391−425.
(6) Poll, L.; Nielsen, G. S.; Varming, C.; Petersen, M. A. Aroma Changes from Raw to Processed Products in Fruits and Vegetables. *Flavour Science - Recent Advances and Trends* **2006**, *43*, 239−244.
(7) Bate, N. J.; Rothstein, S. J. C6-Volatiles Derived from the Lipoxygenase Pathway Induce a Subset of Defense-Related Genes. *Plant J.* **1998**, *16* (5), 561−569.
(8) Gosset, V.; Harmel, N.; Göbel, C.; Francis, F.; Haubruge, E.; Wathelet, J.-P.; Du Jardin, P.; Feussner, I.; Fauconnier, M.-L. Attacks by a Piercing-Sucking Insect (Myzus Persicae Sultzer) or a Chewing Insect (Leptinotarsa Decemlineata Say) on Potato Plants (Solanum Tuberosum L.) Induce Differential Changes in Volatile Compound Release and Oxylipin Synthesis. *J. Exp. Bot.* **2009**, *60* (4), 1231−1240.
(9) Fullana, A.; Carbonell-Barrachina, A. A.; Sidhu, S. Comparison of Volatile Aldehydes Present in the Cooking Fumes of Extra Virgin Olive, Olive, and Canola Oils. *J. Agric. Food Chem.* **2004**, *52* (16), 5207−5214.
(10) Katragadda, H. R.; Fullana, A.; Sidhu, S.; Carbonell-Barrachina, Á. A. Emissions of Volatile Aldehydes from Heated Cooking Oils. *Food Chem.* **2010**, *120* (1), 59−65.
(11) Zhang, Q.; Saleh, A. S.; Chen, J.; Shen, Q. Chemical Alterations Taken Place during Deep-Fat Frying Based on Certain Reaction Products: A Review. *Chem. Phys. Lipids* **2012**, *165* (6), 662−681.
(12) Esposto, S.; Taticchi, A.; Di Maio, I.; Urbani, S.; Veneziani, G.; Selvaggini, R.; Sordini, B.; Servili, M. Effect of an Olive Phenolic Extract on the Quality of Vegetable Oils during Frying. *Food Chem.* **2015**, *176*, 184−192.
(13) Blum, M. S.; Crain, R. D.; Chidester, J. B. Trans-2-Hexenal in the Scent Gland of the Hemipteran Acanthocephala Femorata. *Nature* **1961**, *189* (4760), 245−246.
(14) Arey, J.; Winer, A. M.; Atkinson, R.; Aschmann, S. M.; Long, W. D.; Lynn Morrison, C. The Emission of (Z)-3-Hexen-1-Ol, (Z)-3-Hexenylacetate and Other Oxygenated Hydrocarbons from Agricultural Plant Species. *Atmospheric Environ. Part Gen. Top.* **1991**, *25* (5−6), 1063−1075.
(15) König, G.; Brunda, M.; Puxbaum, H.; Hewitt, C. N.; Duckham, S. C.; Rudolph, J. Relative Contribution of Oxygenated Hydrocarbons to the Total Biogenic VOC Emissions of Selected Mid-European Agricultural and Natural Plant Species. *Atmos. Environ.* **1995**, *29* (8), 861−874.
(16) Kirstine, W.; Galbally, I.; Ye, Y.; Hooper, M. Emissions of Volatile Organic Compounds (Primarily Oxygenated Species) from Pasture. *J. Geophys. Res. Atmospheres* **1998**, *103* (D9), 10605−10619.
(17) Fall, R.; Karl, T.; Hansel, A.; Jordan, A.; Lindinger, W. Volatile Organic Compounds Emitted after Leaf Wounding: On-Line Analysis by Proton-Transfer-Reaction Mass Spectrometry. *J. Geophys. Res. Atmospheres* **1999**, *104* (D13), 15963−15974.
(18) Hatanaka, A.; Harada, T. Formation of Cis-3-Hexenal, Trans-2-Hexenal and Cis-3-Hexenol in Macerated Thea Sinensis Leaves. *Phytochemistry* **1973**, *12* (10), 2341−2346.
(19) Farag, M. A.; Pare, P. W. C6-Green Leaf Volatiles Trigger Local and Systemic VOC Emissions in Tomato. *Phytochemistry* **2002**, *61* (5), 545−554.
(20) Gao, T.; Andino, J. M.; Rivera, C. C.; Márquez, M. F. Rate Constants of the Gas-Phase Reactions of OH Radicals with Trans-2-Hexenal, Trans-2-Octenal, and Trans-2-Nonenal. *Int. J. Chem. Kinet.* **2009**, *41* (7), 483−489.
(21) Jiménez, E.; Lanza, B.; Martínez, E.; Albaladejo, J. Daytime Tropospheric Loss of hexanal and trans-2-hexenal: OH Kinetics and UV Photolysis. *Atmospheric Chem. Phys.* **2007**, *7* (6), 1565−1574.
(22) Davis, M. E.; Gilles, M. K.; Ravishankara, A. R.; Burkholder, J. B. Rate Coefficients for the Reaction of OH with (E)-2-Pentenal,(E)-2-Hexenal, and (E)-2-Heptenal. *Phys. Chem. Chem. Phys.* **2007**, *9* (18), 2240−2248.
(23) Atkinson; Arey, J.; Aschmann, S. M.; Corchnoy, S. B.; Shu, Y. Rate Constants for the Gas-Phase Reactions of Cis-3-Hexen-1-Ol, Cis-3-Hexenylacetate, Trans-2-Hexenal, and Linalool with OH and NO_3 Radicals and O_3 at 296 ± 2 K, and OH Radical Formation Yields from the O_3 Reactions. *Int. J. Chem. Kinet.* **1995**, *27* (10), 941−955.
(24) Kalalian, C.; Samir, B.; Roth, E.; Chakir, A. UV Absorption Spectra of Trans-2-Pentenal, Trans-2-Hexenal and 2-Methyl-2-Pentenal. *Chem. Phys. Lett.* **2019**, *718*, 22−26.
(25) Grira, A.; Antiñolo, M.; Canosa, A.; Tomas, A.; Jiménez, E.; El Dib, G. An Experimental Study of the Gas-Phase Reaction between Cl Atoms and Trans-2-Pentenal: Kinetics, Products and SOA Formation. *Chemosphere* **2021**, *276*, 130193.
(26) Singh, H. B.; Kasting, J. F. Chlorine-Hydrocarbon Photochemistry in the Marine Troposphere and Lower Stratosphere. *J. Atmospheric Chem.* **1988**, *7* (3), 261−285.
(27) Atkinson, R.; Arey, J. Atmospheric Degradation of Volatile Organic Compounds. *Chem. Rev.* **2003**, *103* (12), 4605−4638.
(28) Grosjean, E.; Grosjean, D.; Seinfeld, J. H. Gas-Phase Reaction of Ozone with Trans-2-Hexenal, Trans-2-Hexenyl Acetate, Ethylvinyl Ketone, and 6-Methyl-5-Hepten-2-One. *Int. J. Chem. Kinet.* **1996**, *28* (5), 373−382.
(29) Kalalian, C.; Roth, E.; Chakir, A. Rate Coefficients for the Gas-Phase Reaction of Ozone with C_5 and C_6 Unsaturated Aldehydes. *Int. J. Chem. Kinet.* **2018**, *50* (1), 47−56.
(30) Grosjean, D.; Williams, E. L. Environmental Persistence of Organic Compounds Estimated from Structure-Reactivity and Linear Free-Energy Relationships. Unsaturated Aliphatics. *Atmospheric Environ. Part Gen. Top.* **1992**, *26* (8), 1395−1405.
(31) Cabañas, B.; Salgado, S.; Martín, P.; Baeza, M. T.; Martínez, E. Night-Time Atmospheric Loss Process for Unsaturated Aldehydes: Reaction with NO_3 Radicals. *J. Phys. Chem. A* **2001**, *105* (18), 4440−4445.
(32) Zhao, Z.; Husainy, S.; Smith, G. D. Kinetics Studies of the Gas-Phase Reactions of NO_3 Radicals with Series of 1-Alkenes, Dienes,

https://doi.org/10.1021/acs.jpca.2c05060
J. Phys. Chem. A 2022, 126, 6973−6983

Cycloalkenes, Alkenols, and Alkenals. *J. Phys. Chem. A* **2011**, *115* (44), 12161−12172.
(33) Kerdouci, J.; Picquet-Varrault, B.; Durand-Jolibois, R.; Gaimoz, C.; Doussin, J.-F. An Experimental Study of the Gas-Phase Reactions of NO_3 Radicals with a Series of Unsaturated Aldehydes: Trans-2-Hexenal, Trans-2-Heptenal, and Trans-2-Octenal. *J. Phys. Chem. A* **2012**, *116* (41), 10135−10142.
(34) Rayez, M.-T.; Rayez, J.-C.; Kerdouci, J.; Picquet-Varrault, B. Theoretical Study of the Gas-Phase Reactions of NO_3 Radical with a Series of Trans-2-Unsaturated Aldehydes: From Acrolein to Trans-2-Octenal. *J. Phys. Chem. A* **2014**, *118* (28), 5149−5155.
(35) Albaladejo, J.; Ballesteros, B.; Jiménez, E.; Martín, P.; Martínez, E. A PLP−LIF Kinetic Study of the Atmospheric Reactivity of a Series of C_4−C_7 Saturated and Unsaturated Aliphatic Aldehydes with OH. *Atmos. Environ.* **2002**, *36* (20), 3231−3239.
(36) Rodríguez, D.; Rodríguez, A.; Notario, A.; Aranda, A.; Díaz-de-Mera, Y.; Martínez, E. Kinetic Study of the Gas-Phase Reaction of Atomic Chlorine with a Series of Aldehydes. *Atmospheric Chem. Phys.* **2005**, *5* (12), 3433−3440.
(37) Teruel, M. A.; Achad, M.; Blanco, M. B. Kinetic Study of the Reactions of Cl Atoms with α,β-Unsaturated Carbonyl Compounds at Atmospheric Pressure and Structure Activity Relations (SARs). *Chem. Phys. Lett.* **2009**, *479* (1), 25−29.
(38) Shashikala, K.; Janardanan, D. Degradation Mechanism of Trans-2-Hexenal in the Atmosphere. *Chem. Phys. Lett.* **2020**, *759*, 138039.
(39) Turpin, E.; Tomas, A.; Fittschen, C.; Devolder, P.; Galloo, J.-C. Acetone-H_6 or -D_6 + OH Reaction Products: Evidence for Heterogeneous Formation of Acetic Acid in a Simulation Chamber. *Environ. Sci. Technol.* **2006**, *40* (19), 5956−5961.
(40) Ballesteros, B.; Jiménez, E.; Moreno, A.; Soto, A.; Antiñolo, M.; Albaladejo, J. Atmospheric Fate of Hydrofluoroolefins, $C_xF_{2x+1}CH{=}CH_2$ (x= 1, 2, 3, 4 and 6): Kinetics with Cl Atoms and Products. *Chemosphere* **2017**, *167*, 330−343.
(41) Antiñolo, M.; Asensio, M.; Albaladejo, J.; Jiménez, E. Gas-Phase Reaction of Trans-2-Methyl-2-Butenal with Cl: Kinetics, Gaseous Products, and SOA Formation. *Atmosphere* **2020**, *11* (7), 715.
(42) Ragains, M. L.; Finlayson-Pitts, B. J. Kinetics and Mechanism of the Reaction of Cl Atoms with 2-Methyl-1,3-Butadiene (Isoprene) at 298 K. *J. Phys. Chem. A* **1997**, *101* (8), 1509−1517.
(43) Fantechi, G.; Jensen, N. R.; Saastad, O.; Hjorth, J.; Peeters, J. Reactions of Cl Atoms with Selected VOCs: Kinetics, Products and Mechanisms. *J. Atmospheric Chem.* **1998**, *31* (3), 247−267.
(44) Orlando, J. J.; Tyndall, G. S.; Apel, E. C.; Riemer, D. D.; Paulson, S. E. Rate Coefficients and Mechanisms of the Reaction of Cl-Atoms with a Series of Unsaturated Hydrocarbons under Atmospheric Conditions. *Int. J. Chem. Kinet.* **2003**, *35* (8), 334−353.
(45) Hallquist, M.; Wenger, J. C.; Baltensperger, U.; Rudich, Y.; Simpson, D.; Claeys, M.; Dommen, J.; Donahue, N. M.; George, C.; Goldstein, A. H.; et al. The Formation, Properties and Impact of Secondary Organic Aerosol: Current and Emerging Issues. *Atmos Chem. Phys.* **2009**, *9* (14), 5155−5236.
(46) Antiñolo, M.; del Olmo, R.; Bravo, I.; Albaladejo, J.; Jiménez, E. Tropospheric Fate of Allyl Cyanide ($CH_2{=}CHCH_2CN$): Kinetics, Reaction Products and Secondary Organic Aerosol Formation. *Atmos. Environ.* **2019**, *219*, 117041.
(47) Thévenet, R.; Mellouki, A.; Le Bras, G. Kinetics of OH and Cl Reactions with a Series of Aldehydes. *Int. J. Chem. Kinet.* **2000**, *32* (11), 676−685.
(48) Canosa-Mas, C. E.; Cotter, E. S.; Duffy, J.; Thompson, K. C.; Wayne, R. P. The Reactions of Atomic Chlorine with Acrolein, Methacrolein and Methyl Vinyl Ketone. *Phys. Chem. Chem. Phys.* **2001**, *3* (15), 3075−3084.
(49) Ullerstam, M.; Ljungström, E.; Langer, S. Reactions of Acrolein, Crotonaldehyde and Pivalaldehyde with Cl Atoms: Structure−Activity Relationship and Comparison with OH and NO_3 Reactions. *Phys. Chem. Chem. Phys.* **2001**, *3* (6), 986−992.
(50) Wang, W.; Ezell, M. J.; Ezell, A. A.; Soskin, G.; Finlayson-Pitts, B. J. Rate Constants for the Reactions of Chlorine Atoms with a Series of Unsaturated Aldehydes and Ketones at 298 K: Structure and Reactivity. *Phys. Chem. Chem. Phys.* **2002**, *4* (10), 1824−1831.
(51) Mellouki, A.; Le Bras, G.; Sidebottom, H. Kinetics and Mechanisms of the Oxidation of Oxygenated Organic Compounds in the Gas Phase. *Chem. Rev.* **2003**, *103* (12), 5077−5096.
(52) Orlando, J. J.; Tyndall, G. S. Mechanisms for the Reactions of OH with Two Unsaturated Aldehydes: Crotonaldehyde and Acrolein. *J. Phys. Chem. A* **2002**, *106* (51), 12252−12259.
(53) Wang, D. S.; Ruiz, L. H. Secondary Organic Aerosol from Chlorine-Initiated Oxidation of Isoprene. *Atmospheric Chem. Phys.* **2017**, *17* (22), 13491−13508.
(54) Odum, J. R.; Hoffmann, T.; Bowman, F.; Collins, D.; Flagan, R. C.; Seinfeld, J. H. Gas/Particle Partitioning and Secondary Organic Aerosol Yields. *Environ. Sci. Technol.* **1996**, *30* (8), 2580−2585.
(55) Cai, X.; Griffin, R. J. Secondary Aerosol Formation from the Oxidation of Biogenic Hydrocarbons by Chlorine Atoms. *J. Geophys. Res. Atmospheres* **2006**, *111* (D14), D14206.
(56) Krol, M.; van Leeuwen, P. J.; Lelieveld, J. Global OH Trend Inferred from Methylchloroform Measurements. *J. Geophys. Res. Atmospheres* **1998**, *103* (D9), 10697−10711.
(57) Singh, H. B.; Thakur, A. N.; Chen, Y. E.; Kanakidou, M. Tetrachloroethylene as an Indicator of Low Cl Atom Concentrations in the Troposphere. *Geophys. Res. Lett.* **1996**, *23* (12), 1529−1532.
(58) Finlayson-Pitts, B. J.; Pitts, Jr., J. N. *Chemistry of the Upper and Lower Atmosphere: Theory, Experiments, and Applications*; Elsevier, 2000.
(59) Calvert, J.; et al. *Mechanisms of Atmospheric Oxidation of the Oxygenates*; OUP, 2011.
(60) Spicer, C. W.; Chapman, E. G.; Finlayson-Pitts, B. J.; Plastridge, R. A.; Hubbe, J. M.; Fast, J. D.; Berkowitz, C. M. Unexpectedly High Concentrations of Molecular Chlorine in Coastal Air. *Nature* **1998**, *394* (6691), 353−356.

https://doi.org/10.1021/acs.jpca.2c05060
J. Phys. Chem. A 2022, 126, 6973−6983